SUPPLEMENTAL FIGURES

Supplementary Figure 1

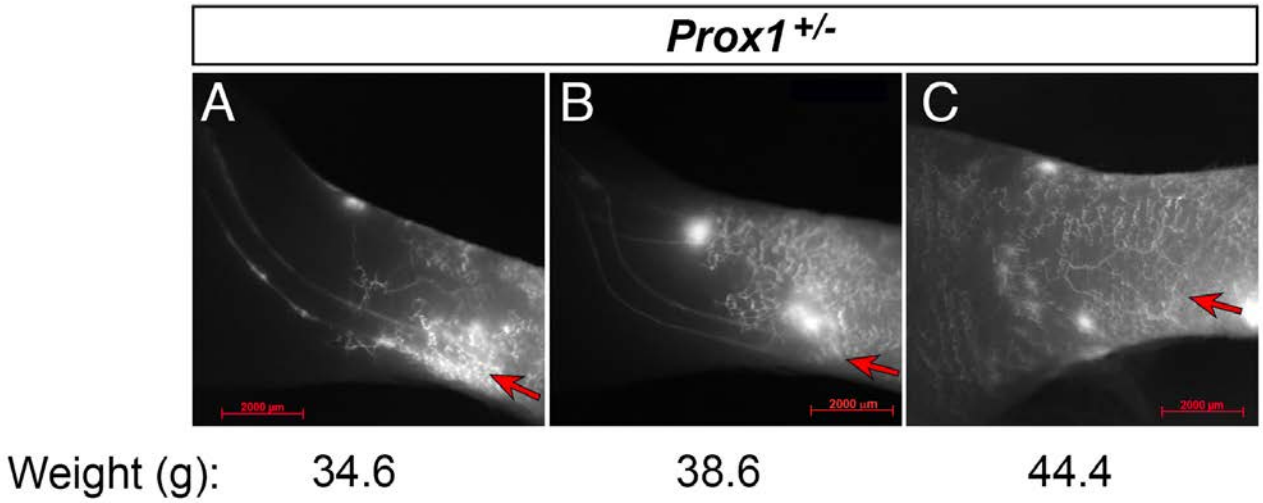

Supplementary Figure 1: Weight appears to correlate with the degree of lymphatic dysfunction in *Prox1*$^{+/-}$ mice.
(A-C) Dynamic NIR fluorescence imaging of 3 younger *Prox1*$^{+/-}$ mice. Red arrows indicate the direction of the flow. Body weight data for each animal is provided below the respective image.

Supplementary Figure 2

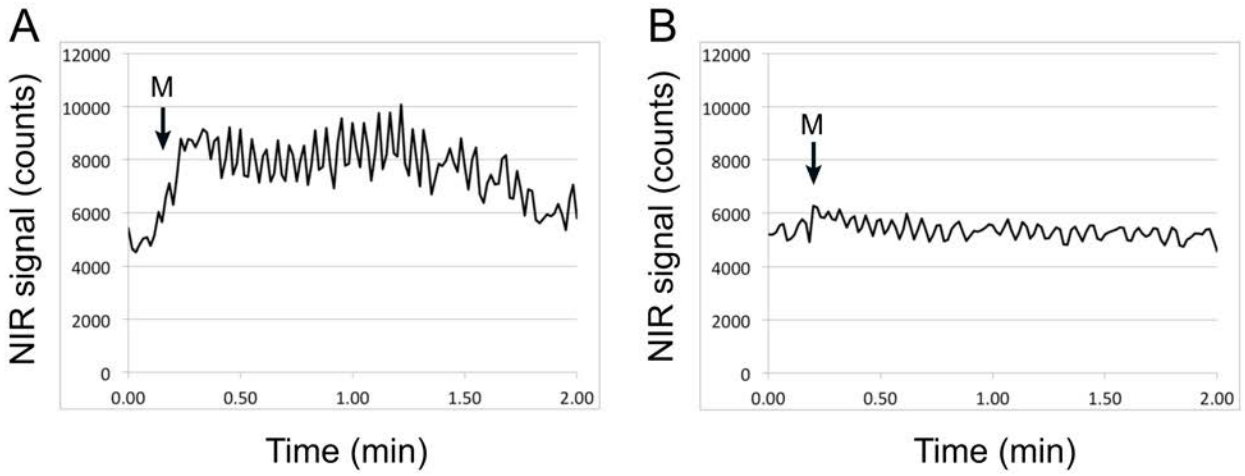

Supplementary Figure 2: Contractility plots from NIR fluorescence imaging of response to mechanostimulation in WT and Prox1$^{+/-}$ mice. (A) Representative response in signal in an afferent collecting lymphatic vessel to mechanostimulation (indicated by arrow) at the site of injection of P20D680 in a young *WT* mouse. (B) Representative response in a young *Prox1*$^{+/-}$ mouse.

Supplementary Figure 3

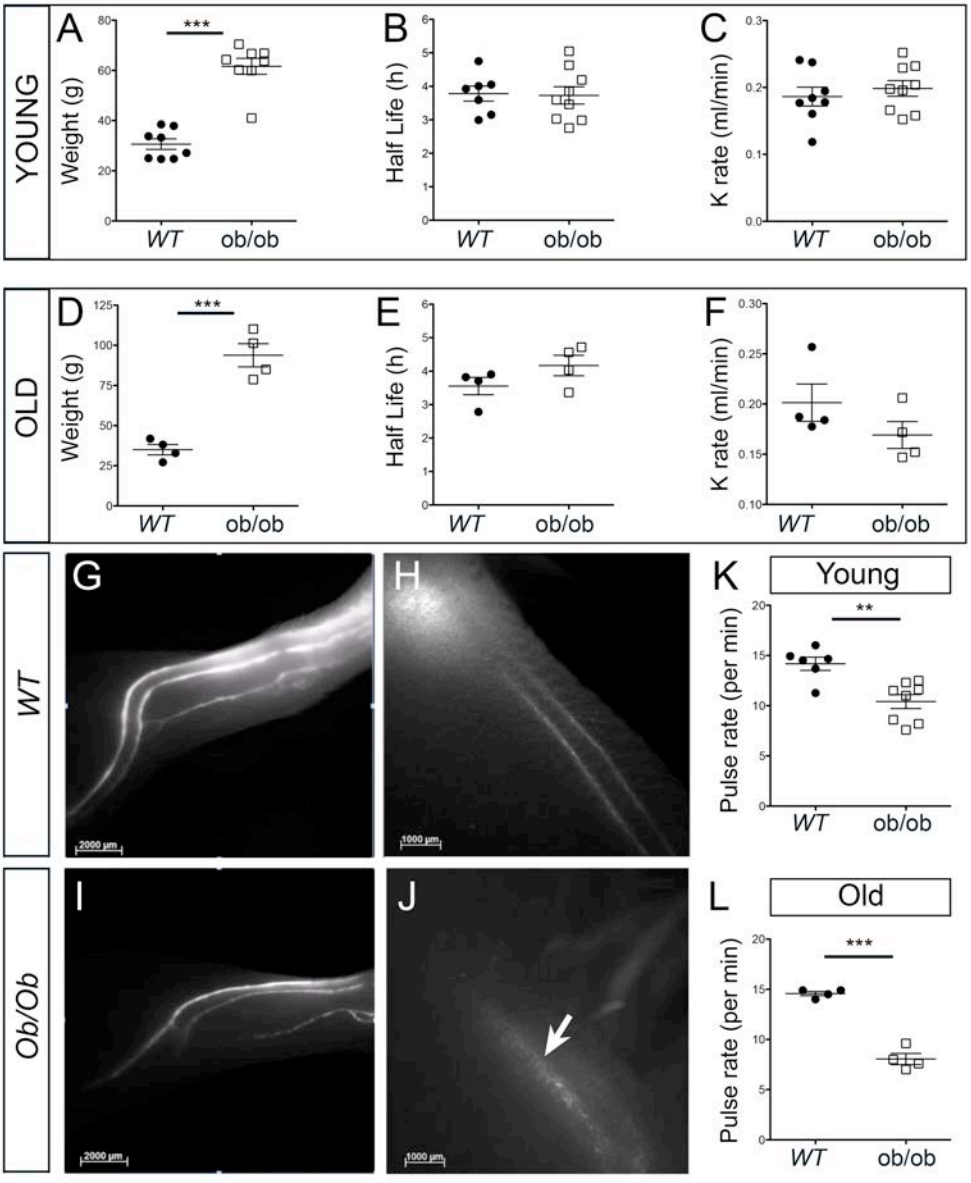

Supplementary Figure 3: Functional analysis of the lymphatic vasculature in Ob/Ob mice. (A, D) Young (A) and old (D) Ob/Ob mice were significantly heavier than their *WT* littermates. (B-C, E-F) However, there were no significantly differences in the half-life (B and E) or clearance rate (C, F) of lymphatic tracer in young (B-C) or old (D-F) Ob/Ob mice. (G-J) Dynamic NIR fluorescence imaging of initial lymphatic vessels showed normal collecting vessels in the lower hindlimb in Ob/Ob mice (I-J). Panels g and i show regions located near the injection sites, and panels H and J show regions close to the popliteal lymph node. No dermal backflow or interstitial leakage was seen in Ob/Ob mice. Some collecting vessels proximal to the popliteal node exhibited dilated vessels (arrow in J) compared with the same region in *WT* (H). (K, L) The frequency of collecting vessel contractions in young (K) and old (L) Ob/Ob mice was less than that in *WT* littermates.
**= p ≤0.01; ***= p ≤0.0001, two-tailed Student's *t*-test.

Supplementary Figure 4

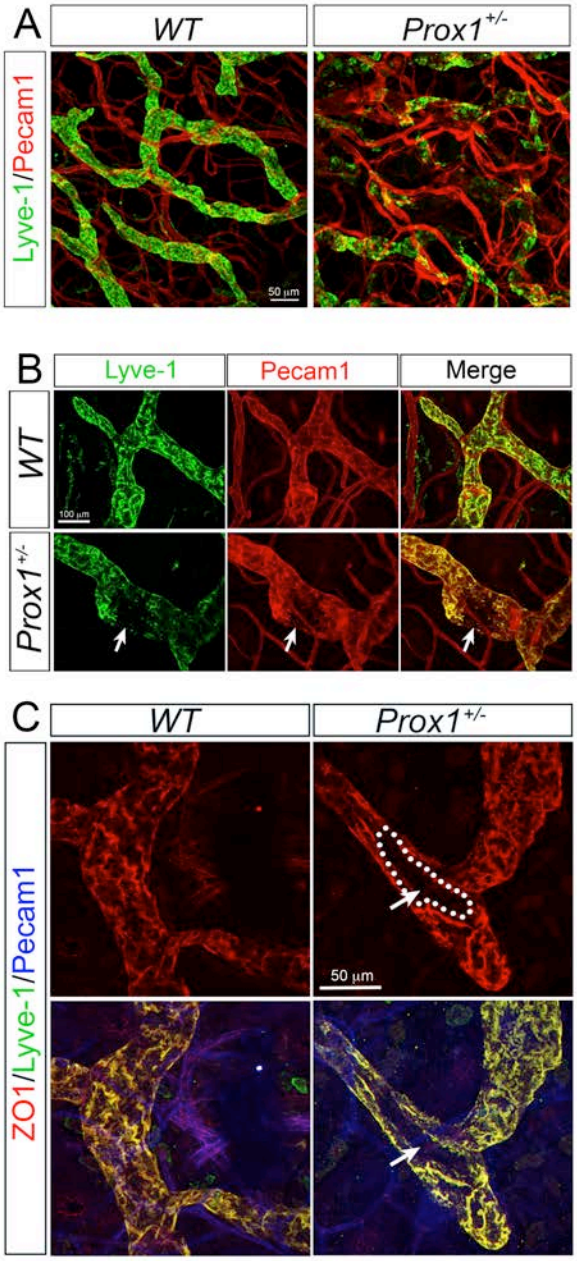

Supplementary Figure 4: Patterning defects in ear lymphatic vessels in *Prox1*$^{+/-}$ mice. (A-B) Whole-mount immunostaining of ears showing the defective lymphatics in 7-week-old *Prox1*$^{+/-}$ mice before the onset of obesity. Lyve-1 (green) staining appeared patchy in *Prox1*$^{+/-}$ mice (A). At higher magnification, the disruption in the structure of the lymphatic vasculature was apparent with the integrity of the lymphatic vessel damaged (B, arrows). (C) Whole-mount immunostaining of dermal lymphatics from 1-month-old *WT* and *Prox1*$^{+/-}$ mice using the endothelial tight junction marker ZO1 highlights the defective lymphatic endothelial cells. Dotted line and arrow indicates lost gap junctions between cells in the single ZO1 channel. Scale bars: 50 μm (A, C) and 100 μm (B).

Supplementary Figure 5

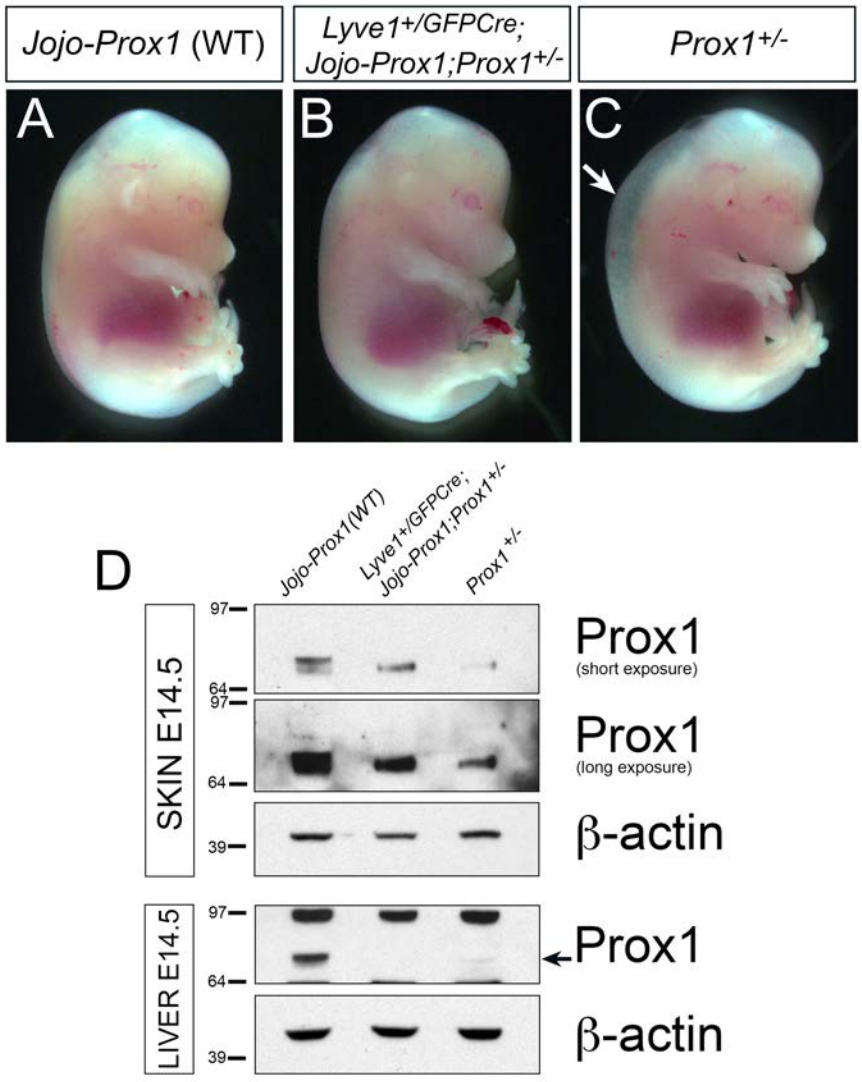

Supplementary Figure 5: Prox1 levels are partially rescued in *Lyve-1$^{+/GFPCre}$;Jojo-Prox1;Prox1$^{+/-}$* mouse embryos. (A-C) At E14.5 and in contrast to Prox1 heterozygous littermates, *Lyve-1$^{+/GFPCre}$;Jojo-Prox1;Prox1$^{+/-}$* do not exhibit edema (B), a characteristic phenotype of *Prox1$^{+/-}$* embryos at this stage (C, arrow). (D) Prox1 levels in embryonic skin (E14.5) were partially rescued in *Lyve-1$^{+/GFPCre}$;Jojo-Prox1;Prox1$^{+/-}$* compared with *Prox1$^{+/-}$* (upper panel). Liver was used as a control tissue where Prox1 is expressed in hepatocytes (bottom panel). Prox1 levels were not restored in *Lyve-1$^{+/GFPCre}$;Jojo-Prox1;Prox1$^{+/-}$* embryos due the absence of Lyve-1 expression.

Supplementary Figure 6

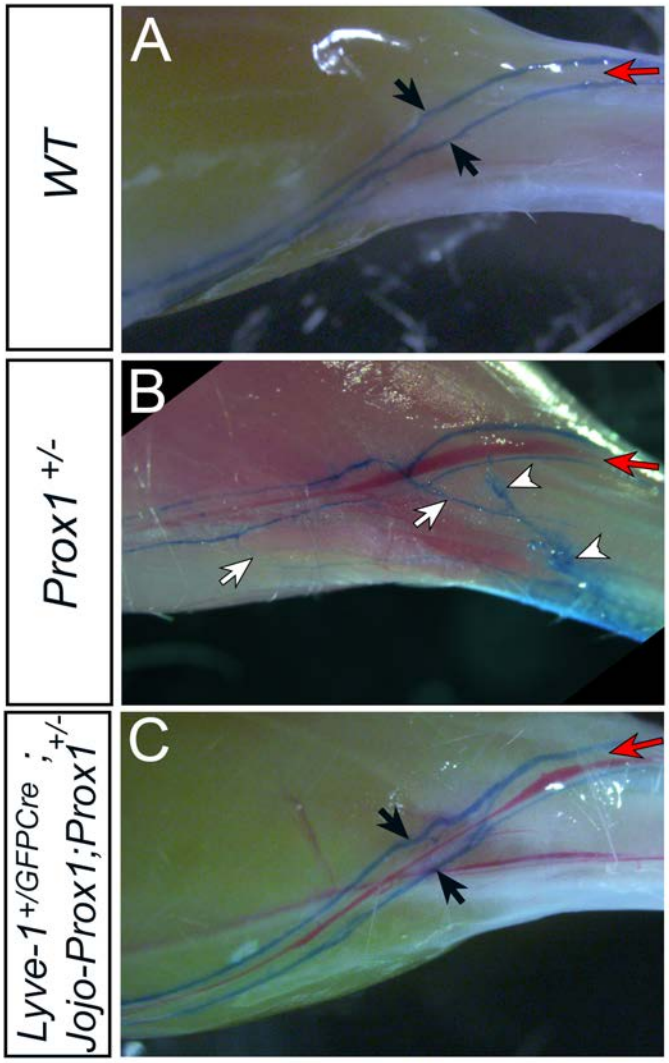

Supplementary Figure 6: Collecting vessels of the lower hindlimbs are normal in *Lyve-1$^{+/GFPCre}$;Jojo-Prox1;Prox1$^{+/-}$* mice

(A-C) Evans blue injections reveal the patterns of the afferent collectors of the lower hind limbs of the indicated genotypes. Representative photographs of mice (aged 4-7 weeks). Black arrows indicate collecting lymphatic vessels; white arrows indicate branches; and white arrowheads indicate leakage points. Red arrows indicate the direction of the flow.

Supplementary Figure 7

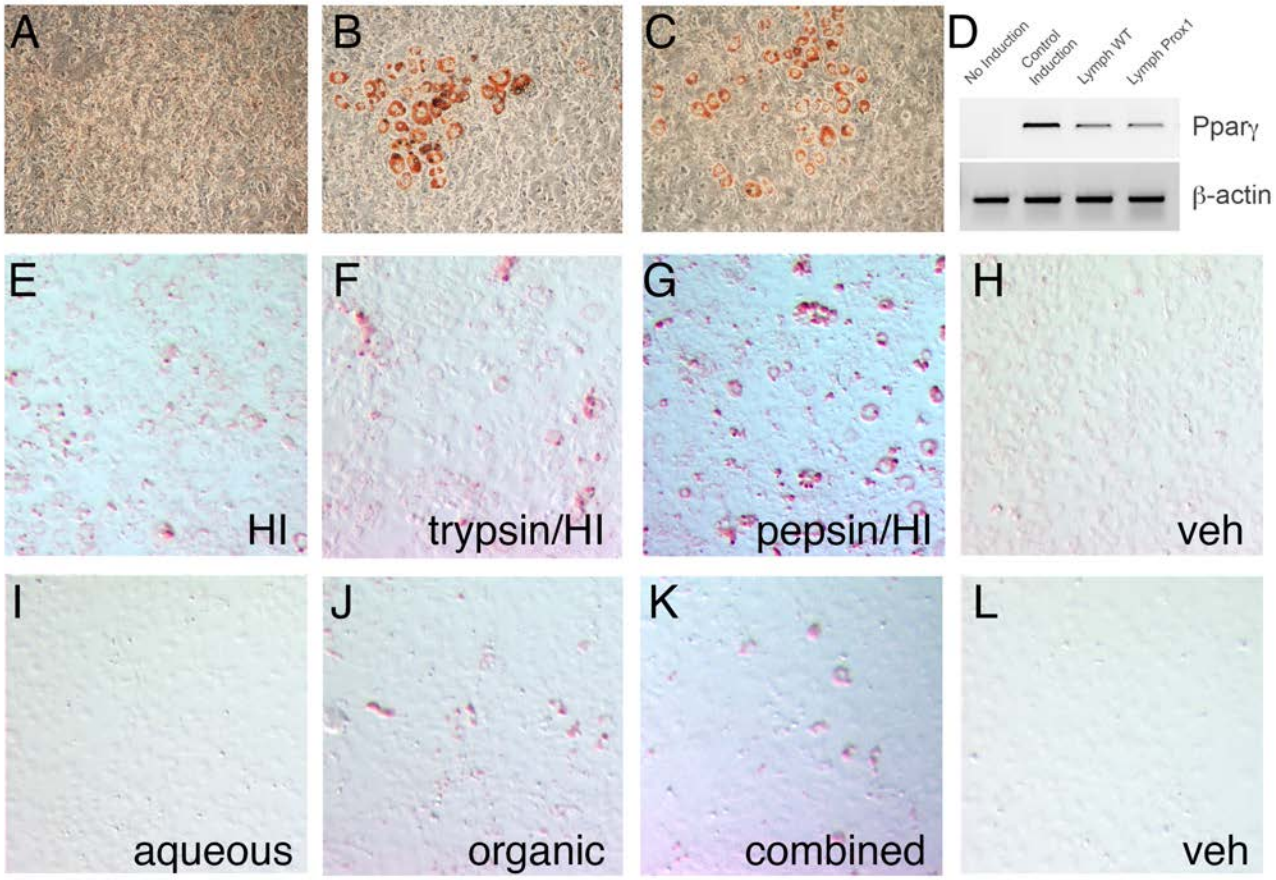

Supplementary Figure 7: The adipogenic factor in chyle is a lipid or group of lipids
(A-C) Lymph from *Prox1*$^{+/-}$ mice and *WT* mice were equally adipogenic. In vitro adipogenic studies of 3T3-L1 preadipocytes showed Oil-Red-O accumulation was equivalent when cells were exposed to lymph from *Prox1*$^{+/-}$ (B) or *WT* (C) mice. (D) RT-PCR analysis for Pparγ and β-actin. (E-H) The adipogenic factor in chyle was not a protein. Isolated chyle was subjected to heat inactivation alone (E) or with subsequent protease treatment (F, G) to denature the proteins. Adipocytes exposed to the treated chyle still showed substantial Oil-Red-O staining. (I-L) The organic phase of chyle was adipogenic. The Bligh-Dyer method was used to separate chyle lipids and proteins into organic and aqueous phases, respectively. The aqueous phase, containing most proteins, was not adipogenic (I), but the organic phase (J) and the combined organic and aqueous phases (K) showed substantial Oil-Red-O staining. Abbreviations: HI, heat inactivation; veh, vehicle.

Supplemental Video Legends

Video 1. Typical lymphatic perfusion pattern in a WT mouse. Injection of 5 µL of 20 µmol/L P20D680 into dorsal skin of the rear paw leads to perfusion of collecting lymphatic vessels in the lower limb. Video is 5x normal speed.

Video 2. Typical lymphatic perfusion pattern in a *Prox1*$^{+/-}$ mouse. Injection of 5 µL of 20 µmol/L P20D680 into dorsal skin of the rear paw leads to perfusion of collecting lymphatic vessels in the lower limb with extensive dermal backflow immediately apparent. Video is 5x normal speed.